Early members of 'living fossil' lineage imply later origin of modern ray-finned fishes

Giles, Sam; Xu, Guang-Hui; Near, Tom; Friedman, Matt

DOI:
10.1038/nature23654

License:
Other (please specify with Rights Statement)

Document Version
Peer reviewed version

Citation for published version (Harvard):
Giles, S, Xu, G-H, Near, T & Friedman, M 2017, 'Early members of 'living fossil' lineage imply later origin of modern ray-finned fishes', *Nature*, vol. 549, no. 7671, pp. 265–268. https://doi.org/10.1038/nature23654

Early members of 'living fossil' lineage imply later origin of modern ray-finned fishes

Sam Giles[1]*, Guang-Hui Xu[2], Thomas J. Near[3], Matt Friedman[1,4]

[1]Department of Earth Sciences, University of Oxford, South Parks Road, Oxford, OX1 3AN, UK.

[2] Key Laboratory of Vertebrate Evolution and Human Origins of Chinese Academy of Sciences, Institute of Vertebrate Paleontology and Paleoanthropology, Chinese Academy of Sciences, Beijing 100044, China

[3]Department of Ecology & Evolutionary Biology and Peabody Museum of Natural History, Yale University, 165 Prospect St, New Haven, CT 06520, USA

[4]Museum of Paleontology and Department of Earth and Environmental Sciences, University of Michigan, 1109 Geddes Ave, Ann Arbor, MI 48109, USA

*Corresponding author. E-mail: sam.giles@earth.ox.ac.uk

Modern ray-finned fishes (Actinopterygii) comprise half of extant vertebrate species and are widely thought to have originated before or near the end of the Middle Devonian (~385 million years (Myr) ago)[1-4]. Polypterids (bichirs and ropefish) represent the earliest-diverging lineage of living actinopterygians, with almost all Palaeozoic taxa interpreted as more closely related to other extant actinopterygians than to polypterids[5-10]. By contrast, the earliest material

assigned to the polypterid lineage is mid-Cretaceous (ca. 100 Mya) in age[11], implying a quarter-of-a-billion-year palaeontological gap. We show that scanilepiforms, a widely distributed Triassic (ca. 252-201 Mya) radiation, are stem polypterids. Significantly, these fossils break the long polypterid branch and expose many supposedly primitive features of extant polypterids as reversals. This shifts numerous Palaeozoic ray-fins to the actinopterygian stem, reducing the minimum age for the crown lineage by roughly 45 Myr. Recalibration of molecular clocks to exclude phylogenetically reassigned Palaeozoic taxa results in age estimates for the actinopterygian crown lineage ~20–40 million years younger than previous molecular analyses[1-4]. These new dates are broadly consistent with our revised palaeontological timescale and coincident with an interval of conspicuous morphological and taxonomic diversification among ray-fins centred on the Devonian-Carboniferous boundary[12-14]. A shifting timescale, combined with ambiguity in the relationships of late Palaeozoic actinopterygians, highlights this part of the fossil record as a major frontier in understanding the evolutionary assembly of modern vertebrate diversity.

The roughly dozen living species of polypterids have long vexed vertebrate biologists[15]. These freshwater, African endemics were only recognized as ray-finned fishes in the early 20th century[16,17], although this view was resisted by some until the 1970s[18]. Anatomical and molecular data now support placement of polypterids as the living sister group of all other extant actinopterygians[1-7,9,19]. Morphological analyses generally resolve polypterids as one of the earliest diverging ray-finned lineages, with only the Middle-Late Devonian *Cheirolepis* consistently falling on the

actinopterygian stem[5-7,9,20]. Despite apparently ancient evolutionary origins and perceived status as 'living fossils'[15], polypterids have a meagre palaeontological record consisting largely of fragments[10,11]. The oldest polypterids are mid-Cretaceous in age[21], postdating the predicted origin of the lineage by at least 285 Myr, and show few differences from modern species[17,22,23], which originated in the Miocene (ca. 20 Myr[15]). The lack of specializations found in early representatives of other living ray-fin groups suggests an ancient origin for polypterids, but several of these absences concern distinctive aspects of polypterid morphology that do not closely resemble the anatomy of the oldest ray-finned fishes[10,15]. Fossils have played an important role in establishing relationships among living actinopterygian lineages[16,19], so the lack of early polypterids leaves an outstanding gap in our understanding of the evolutionary history of this group and of vertebrates more generally.

Scanilepiformes is a widespread group of Triassic 'palaeoniscoid' fishes known from continental or marginal marine deposits in Sweden, Russia, China, Kyrgyzstan and the United States. Links between scanilepiforms and polypterids have been made based on morphological similarity, referencing a mix of ancestral (e.g., large gular plates) and derived, but homoplastic (e.g., long-based dorsal fin), characters[24-25]. However, past cladistic analyses resolve scanilepiforms as actinopterans, specifically stem-group neopterygians[9,26], rejecting a close phylogenetic relationship with polypterids.

Most scanilepiform fossils are heavily compressed, limiting investigations to external anatomy. The Middle Triassic *Fukangichthys* represents an important exception (Fig. 1, Extended Data Figures 1–3). High-resolution micro-computed tomography (μCT)

of three-dimensionally preserved skulls illuminates internal cranial anatomy of scanilepiforms. The trough-shaped interorbital walls, which do not contact at the midline (Fig. 1c and Extended Data Figure 1c), are separated from the weakly ossified otic and occipital regions of the neurocranium (Extended Data Figure 1a). The optic foramen is ventrally positioned, and the parasphenoid contributes to its lower margin (Fig. 1b,c and Extended Data Figure 1b,c). The parasphenoid has long but simple ascending processes, a triangular corpus pierced by a hypophysial canal, and no posterior stalk (Fig. 1b,e and Extended Data Figure 1b,e). A small median vomer lies anterior to the parasphenoid (Fig. 1e and Extended Data Figure 1e). Dermal bones on the inner surface of the palate include the accessory vomer, dermetapterygoid, three dermopalatines, entopterygoid, and an ectopterygoid bearing a lateral process that articulates with the inner face of the maxilla (Fig. 1e and Extended Data Figures 1e, 4). Like the maxilla and premaxilla, the dentary bears a single row of peg-like teeth. The hook-shaped coronoid process is composed exclusively of the prearticular (Fig. 1b and Extended Data Figures 1a, 4e). A modest opercular process extends from the 'L'-shaped hyomandibula, which is imperforate and unfused to the dermohyal (Fig. 1b and Extended Data Figure 1b). Plate-like ceratohyals, which bear a groove for the afferent hyoid artery, flank the four pairs of ceratobranchials and hypobranchials (Fig. 1d and Extended Data Figures 1d, 5). Epibranchials bear uncinate processes, and multiple basibranchial ossifications may be present (Fig. 1d and Extended Data Figures 1d, 5).

We conducted a revised analysis of actinopterygian interrelationships based on an expanded morphological dataset[27] (93 taxa, 265 characters), and an analysis of this morphological dataset combined with DNA sequences of 12 nuclear genes.

Phylogenies were inferred using both parsimony (Fig. 2 and Extended Data Figures 6, 7) and Bayesian methods (Extended Data Figure 8). In contrast to some, but not all[28-29], previous studies, we have rooted our analyses on a set of non-actinopterygian outgroups, rather than *Cheirolepis*[6,9,26] or a hypothetical ancestor[7,20]. With respect to living actinopterygians alone, we corroborate the placement of chondrosteans and polypterids as successively more remote outgroups to neopterygians (Fig. 2 and Extended Data Figures 6–8)[1-10,26,28], although this resolution is lost in phylogenies inferred by Bayesian analysis of morphological data (Extended Data Figure 8B). With respect to fossil taxa alone, our results are congruent with previous studies: an early diverging assemblage of Devonian taxa, a grade of 'palaeoniscoid' lineages arising in the later Palaeozoic, and a series of early Mesozoic 'subholostean' taxa branching immediately outside of crown Neopterygii[1,6-7,9,26].

Where our results differ substantially from the generally accepted pattern of actinopterygian diversification is in the intersection of relationships between living and fossil taxa. Polypterids are nested within scanilepiforms, and numerous Devonian–Triassic taxa previously interpreted as crown actinopterygians are resolved as stem-lineage ray-finned fishes. Consequently, a late Middle or early Late Devonian (ca. 385-378 Ma;[1,5-7,9]) minimum for the actinopterygian crown is not supported (successive nodes excluding Devonian taxa from crown: BPPs in morphology analysis = 0.83, 0.69; BPPs in combined analysis = 0.96, 0.83; Bremer decay indices = 2, 2, 4, 2). The crown node is subtended by a polytomy in the Bayesian analyses, creating ambiguity as to a revised minimum age of actinopterygians. However, no resolution is compatible with a minimum older than Viséan, some 45 million years younger than currently held[1-4,30].

The monophyly of polypterids plus scanilepiforms is strongly supported (BPP = 0.98-0.92; Bremer decay index = 4) and rests on features distributed throughout the skeleton, including: optic foramen adjacent to dorsal margin of parasphenoid; broad interorbital septum; lateral process of the ectopterygoid[19]; four ceratobranchials[31]; loss of fulcra along dorsal ridge of caudal fin; and coronoid process of the lower jaw composed exclusively of the prearticular (Supplementary Information and Supplementary Figure 1).

This revised placement of scanilepiforms indicates that many apparently primitive features of polypterids are reversals. These include traits also absent in other living actinopterygian lineages, but long recognized as parallel losses through identification of early fossil members of those groups: fringing fulcra (retained only by gars), a surangular (retained only by holosteans), a spiracular canal (retained only by chondrosteans and holosteans), and a lateral cranial canal (retained only by chondrosteans and gars). We note that the cranial endocavity of *Erpetoichthys* bears short lateral diverticulae aligned with the posterior semicircular canal, possibly representing a vestigial lateral cranial canal (Extended Data Figure 9). Additional features previously cited as evidence for an especially deep divergence of polypterids within actinopterygian phylogeny do not closely match either generalised osteichthyan or derived actinopteran conditions, but in fact are best described as a third, probably autapomorphic, state. This is particularly apparent in the pectoral-fin skeleton of polypterids, which is coded identically to that of *Cheirolepis* in many analyses[6-7,9], but which shows a highly specialized architecture[18].

Revised paleontological minima for deep actinopterygian divergences could alter the inferred timeline of actinopterygian evolution[1-4,10]. To assess the temporal implications of new fossil placements, we conducted two parallel relaxed molecular clock analyses. We utilized previously proposed paleontological constraints[2,4,31], but varied application of actinopterygian calibrations of Palaeozoic and earliest Mesozoic ages. The first analysis employed constraints in line with past interpretations of early actinopterygian phylogeny[1-4]. Our second analysis excluded these calibrations entirely, relying on well-established minima for outgroups and nested ray-fin clades to estimate the timing of early actinopterygian divergences via interpolation. We have not assigned new calibrations to these deep nodes for three reasons. First, a lack of consistent resolution across our trees hinders the identification of specific minima. Second, phylogenetic leaf stability of Carboniferous-Early Triassic actinopterygians is substantially lower than that of either stratigraphically earlier or later forms (Fig. 3; although scanilepiforms are relatively stable). When adjusted for taxonomic incompleteness, Early Triassic taxa perform particularly poorly (Fig. 3b). The variable positions of many Carboniferous-Early Triassic taxa across the actinopteran, neopterygian and chondrostean stems in our analyses (Extended Data Figures 6 and 8) questions the reliable identification of calibrations at present. Third, and most significantly, interpolated—as opposed to directly calibrated—node-age estimates for these deep divergences provide an independent assessment of the two competing age models for the actinopterygian crown clade: evolution deep within the Devonian, or a later origin in the Carboniferous as suggested by our new phylogenetic results.

The two analyses deliver largely non-overlapping ages for the actinopterygian crown node (Supplementary Table 1): use of all calibrations results in a late Emsian-earliest

Frasnian estimate (mean: 389.9 Ma [Eifelian]; 95% HPD: 382.6, 397.8 Ma), while the restricted calibration set yields a much younger estimate, latest Givetian-Viséan (mean: 359.6 Ma [terminal Famennian]; 95% HPD: 335.5-384.1 Ma). This younger age estimate cannot reject crown-group membership for the Devonian *Mimipiscis* and *Moythomasia*[30] on temporal grounds, but they lie far within the oldest tail of the posterior age distribution. By contrast, this molecular age estimate closely matches a first palaeontological appearance of crown lineage actinopterygians in the Mississippian, even though these fossils were not used as calibrations in the relaxed molecular clock analyses. The divergence between mean age estimates under these two calibration strategies differs by approximately 30 Myr, corresponding roughly to the difference between palaeontological minima for the actinopterygian crown indicated by past studies[2-3] and our own results. Our revised timescale places the origin of the modern ray-finned fishes near the Devonian-Carboniferous boundary, after which considerable taxonomic and morphological diversification is apparent in the actinopterygian fossil record[8,10,12-14]. This supports an emerging view of the early Carboniferous as a critical interval in establishment of key modern vertebrate radiations.

References

1. Hurley, I. A. et al. A new time-scale for ray-finned fish evolution. *Proc. Biol. Sci.* 274, 489–498 (2007).
2. Near, T. J. et al. Resolution of ray-finned fish phylogeny and timing of diversification. *Proc. Natl Acad. Sci.* USA 109, 13698–13703 (2012).

3. Broughton, R. E., Betancur-R, R., Li, C., Arratia, G. & Ortí, G. Multi-locus phylogenetic analysis reveals the pattern and tempo of bony fish evolution. *PLoS Curr.* doi:10.1371/currents.tol.2ca8041495ffafd0c92756e75247483e (16 April 2013).
4. Faircloth, B. C., Sorenson, L., Santini, F. & Alfaro, M. E. A phylogenomic perspective on the radiation of ray-finned fishes based upon targeted sequencing of ultraconserved elements (UCEs). *PLoS One* 8, e65923 (2013).
5. Patterson, C. Morphology and interrelationships of primitive actinopterygian fishes. *Am. Zool.* 22, 241–295 (1982).
6. Gardiner, B. G. The relationships of the palaeoniscid fishes, a review based on new specimens of *Mimia* and *Moythomasia* from the Upper Devonian of Western Australia. *Bull. Br. Mus. Nat. Hist.* 37, 173–428 (1984).
7. Coates, M. I. Endocranial preservation of a Carboniferous actinopterygian from Lancashire, UK, and the interrelationships of primitive actinopterygians. *Philos. Trans. R. Soc. London Biol.* 354, 435–462 (1999).
8. Sallan, L. C. Major issues in the origins of ray-finned fish (Actinopterygii) biodiversity. *Biol. Rev. Camb. Philos. Soc.* 89, 950–971 (2014).
9. Xu, G. H., Gao, K. Q. & Finarelli, J. A. A revision of the Middle Triassic scanilepiform fish *Fukangichthys longidorsalis* from Xinjiang, China, with comments on the phylogeny of the Actinopteri. *J. Vertebr. Paleontol.* 34, 747–759 (2014).
10. Friedman, M. The early evolution of ray-finned fishes. *Palaeontology* 58, 213–228 (2015).

11. Gayet, M., Meunier, F. J. & Werner, C. Diversification in Polypteriformes and special comparison with the Lepisosteiformes. *Palaeontology* 45, 361–376 (2002).
12. Sallan, L. C. & Coates, M. I. Styracopterid (Actinopterygii) ontogeny and the multiple origins of post-Hangenburg deep bodied fishes. *Zool. J. Linnean. Soc.* 169, 156–199 (2013).
13. Sallan, L.C. & Friedman, M. Heads or tails: staged diversification in vertebrate evolutionary radiations. *Proc. Biol. Soc* 279, doi: 101098/rspb.2011.2454.
14. Friedman, M. & Sallan, L. C. Five hundred million years of extinction and recovery: a Phanerozoic survey of large-scale diversity patterns in fishes. *Palaeontology* 55,707–742 (2012).
15. Near et al. Boom and bust: ancient and recent diversification in bichirs (Polypteridae: Actinopterygii), a relictual lineage of ray-finned fishes. *Evolution* 68,1014–1026 (2013).
16. Goodrich, E. S. *Polypterus*, a palaeoniscid? *Palaeobiologica* 1, 87–91 (1928).
17. Allis, E. P. The cranial anatomy of *Polypterus*, with special reference to *Polypterus bichir*. *J. Anat.* 56, 189–294 (1922).
18. Jessen, H. L. *In Interrelationships of Fishes* (eds Greenwood, P. H., Miles, R. S. & Patterson, C.), 63–103 (Academic, 1973).
19. Grande, L. An empirical synthetic pattern study of gars (Lepisosteiformes) and closely related species, based mostly on skeletal anatomy. The resurrection of Holostei. *American Society of Ichthyologists and Herpetologists, Special Publication* 6, 1–871 (2010).

20. Gardiner, B. G., Schaeffer, B. & Masserie, J. A. A review of the lower actinopterygian phylogeny. *Zool. J. Linnean. Soc.* 144, 511–525 (2005).
21. Duthiel, D. B. The first articulated fossil cladistian: *Serenoichthys kemkemensis*, gen. et sp. nov., from the Cretaceous of Morocco. *J. Vertebr. Paleontol.* 19, 243 – 246 (1999).
22. Jollie, M. Development of the head and pectoral skeleton of *Polypterus* with a note on scales (Pisces: Actinopterygii). *J. Zool.* 204, 469–507 (1984).
23. Claeson, K., Bemis, W. E. & Hagadorn, J. W. New interpretations of the skull of a primitive bony fish *Erpetoichthys calabaricus* (Actinopterygii: Cladistia). *J. Morphol.* 268, 1021–1039 (2007).
24. Selezneva, A. A. *Evenkia* — Ancestor of *Polypterus* (Actinopterygii). *Paleontological Journal* 19, 1–6 (1985).
25. Sytchevskaya, E. K. In *Mesozoic Fishes 2. Systematics and Fossil Record* (eds Arratia, G. & Schultze H.-P.) 445–468 (Dr. Friedrich Pfeil, 1999).
26. Xu, G.-H. & Gao, K.-Q. A new scanilepiform from the Lower Triassic of northern Gansu Province, China, and the phylogenetic relationships of non-teleostean Actinopterygii. *Zool. J. Linnean. Soc.* 161, 595–612 (2011).
27. Giles, S., Darras, L., Clément, G., Blieck, A. & Friedman, M. An exceptionally preserved Late Devonian actinopterygian provides a new model for primitive cranial anatomy in ray-finned fishes. *Proc. Biol. Sci.* 282, 20151485 (2011).
28. Cloutier, R. & Arratia, G. In *Recent Advances in the Origin and Early Radiation of Vertebrates* (eds Arratia, G., Wilson, M. H. V. & Cloutier, R.) 217–270 (Verlag Dr. Friedrich, 2004).

29. Mickle, K. E., Lund, R. & Grogan, E. D. Three new palaeoniscoid fishes from the Bear Gulch Limestone (Serpukhovian, Mississippian) of Montana (USA) and the relationships of lower actinopterygians. *Geodiversitas* 31, 623–668 (2009).
30. Benton, M. J. et al. Constraints on the timescale of animal evolutionary history. *Palaeo. Electronica* 18.1.1FC (2015).
31. Britz, R. & Johnson, G. D. On the homology of the posteriormost gill arch in polypterids (Cladistia, Actinopterygii). *Zool. J. Linnean. Soc.* 138, 495–503 (2011).
32. Giles, S. Xu, G.-H., Near, T. J. & Friedman, M. *Fukangichthys*: CT scan data and surface files from middle Triassic fossil scanilepiform fish. figshare. https://doi.org/10.6084/m9.figshare.c.3814360 (2017).

Main Text Figure Legends

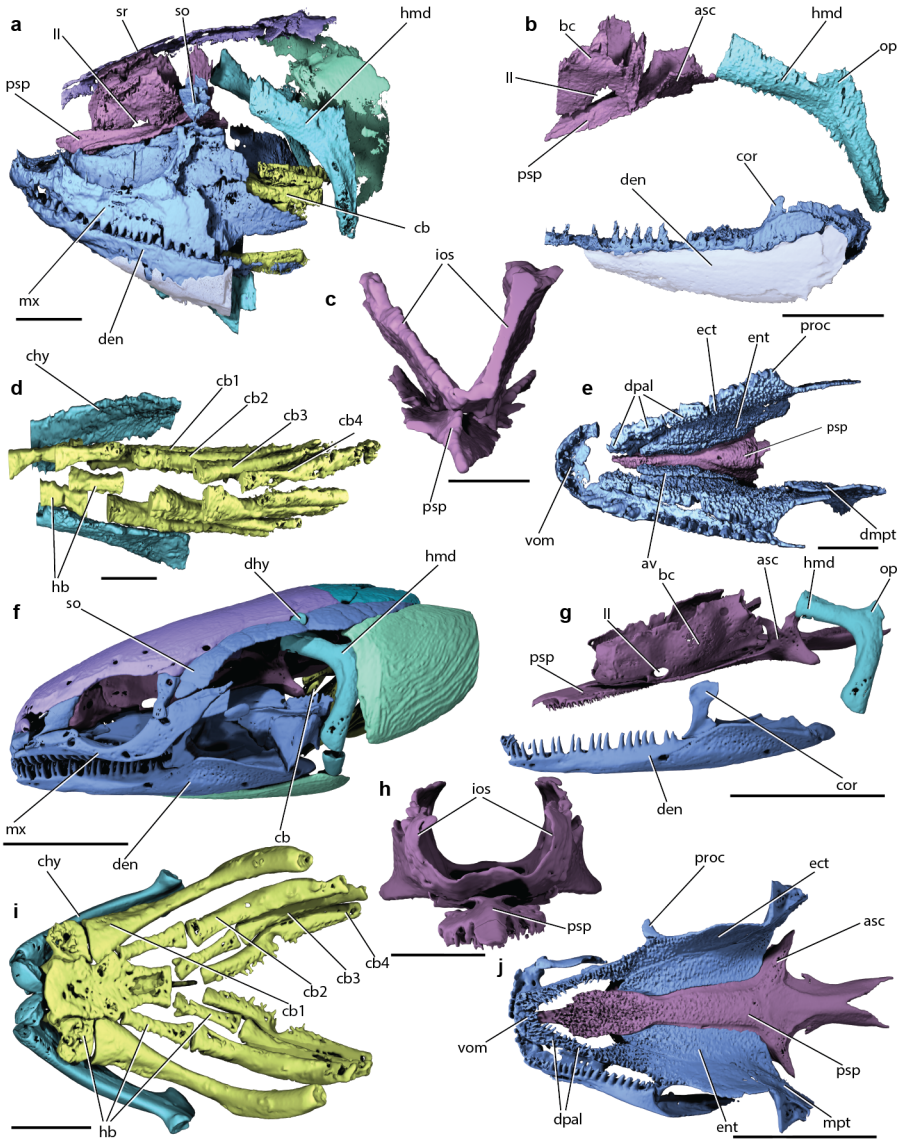

285

286 **Figure 1 | Comparative cranial anatomy of *Fukangichthys longidorsalis* (IVPP**

287 **V4096.6 and IVPP V4096.13; a-e) and *Erpetoichthys calabaricus* (BMNH**

288 **2016.9.22.3**; **f-j) based on high-resolution computed tomography. a,f,** Lateral view

289 of whole skull (**a**: IVPP V4096.6). **b,g,** Lateral view of braincase, hyomandibula and

290 lower jaw (**b**: IVPP V4096.13). **c,h,** Braincase in anterior view (**c**: IVPP V4096.13).

291 **d,i,** Ventral portions of hyoid and branchial arches in dorsal view (**d**: IVPP V4096.6).

292 **e,j,** Upper jaws and palate in ventral view (**e**: IVPP V4096.6). Abbreviations: asc,

293 parasphenoid ascending process; av, accessory vomer; bc, braincase; cb,

294 ceratobranchial; chy, ceratohyal; cor, coronoid process; den, dentary; dmpt,

dermetapterygoid; dpal, dermopalatine; ect, ectopterygoid; ent, entopterygoid; hb, hypobranchial; hmd, hyomandibula; ios, interorbital septa; mpt, metapterygoid; mx, maxilla; op, opercular process; proc, ectopterygoid process; psp, parasphenoid; so, suborbitals; vom, median vomer; II, optic foramen. Mouldic portion of lower jaw shaded. Colour coding of skeletal elements: blue, cheek and jaw; purple, skull roof; mauve, braincase and parasphenoid; light blue, hyoid arch; green, operculogular system; turquoise, shoulder girdle; yellow, gill skeleton. Interpretive drawings shown in Extended Data Figure 3. Scale bar, 5 mm in **a-b,e-g,j**, 2mm in **c-d,h-i**.

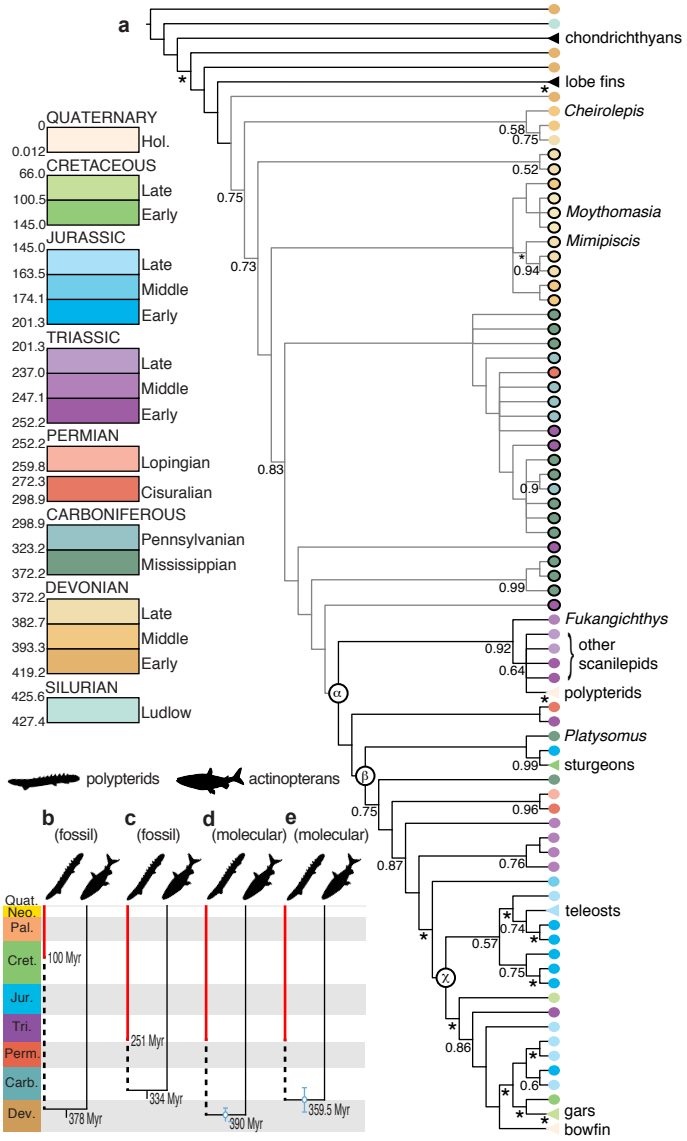

Figure 2 | Phylogenetic results and implications for polypterid total group and actinopterygian crown group. **a**, Summary of strict consensus tree. Some clades collapsed or omitted and some taxon names removed. Circles indicate fossils; triangles extant radiations. Grey branches indicate stem-lineage actinopterygians; outlined terminals indicate taxa previously hypothesised to be crown Actinopterygii (refs 6-7, 9, 26) but resolved as stem Actinopterygii here. Numbers at nodes represent Bayesian posterior probabilities (where the same nodes are resolved in common across all analyses); asterisk indicates BPP of 1. α: crown Actinopterygii; β: crown Actinopteri; χ: crown Neopterygii. Full cladograms provided in Extended Data Figure 6. Previous (**b**) and revised (**c–e**) timescales of polypterid and actinopterygian evolution. Fossil timescales are derived from the stratigraphically oldest taxa within the crown: *Mimpiscis* and *Moythomasia* (~378 Myr) in (**b**), (conservatively based on refs 6-7, 9, 26, 30); *Platysomus* (~334 Myr) in (**c**), based on this analysis. Molecular clock timescales derived from this analysis with (**d**) and without (**e**) Palaeozoic-Triassic actinopterygian calibrations. Red line indicates polypterid fossil record, black dashed line indicates polypterid ghost lineage. Error bars represent 95% credible intervals.

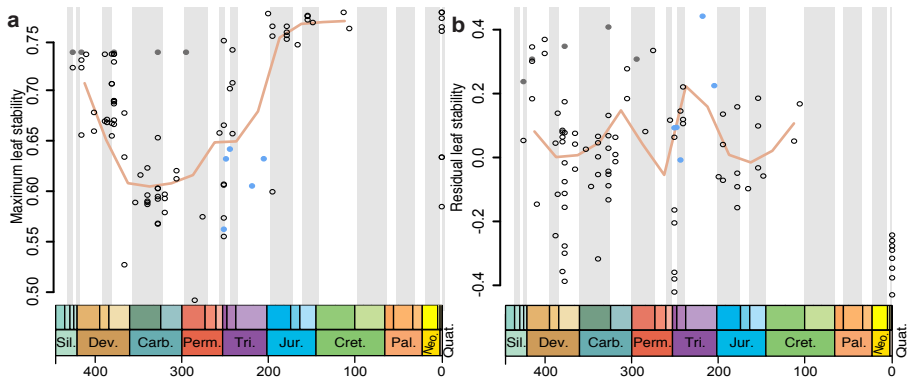

Figure 3 | Measures of taxon stability. a, Raw leaf stability plotted against taxon age. **b,** Residuals from a linear regression of stability against taxon incompleteness, plotted against taxon age. Taxa identified in Extended Data Figure 10 and Supplementary Table 2. Blue circles represent scanilepiforms. Grey circles represent taxa constrained to the outgroup during phylogenetic analyses. Orange line shows moving average.

Supplementary Information is linked to the online version of the paper at www.nature.com/nature.

Acknowledgements

Y.-M. Hou, D. Sykes and R. Summerfield assisted with CT scanning. C. Healy, Z. Johanson and M.M. Smith provided scans of *Erpetoichthys*. L. Sallan provided helpful discussion. N. Brocklehurst aided with R, and L. Parry assisted with R and Mr Bayes. S.G. was supported by a Junior Research Fellowship from Christ Church, Oxford, and a L'Oréal-UNESCO For Women in Science Fellowship. G.-H.X. was supported by the National Natural Science Foundation of China (41672001). T.J.N was supported by the National Science Foundation (ANT-134166) and the Bingham Oceanographic Fund from the Peabody Museum of Natural History, Yale University. M.F was supported by a Philip Leverhulme Prize (PLP-2012-130) and Leverhulme Trust Project Grant (RPG-2012-65A).

Author Contributions

The project was conceived by M.F. CT scanning was carried out by S.G., G.-H. X. and M.F. S.G. segmented the CT data, conducted phylogenetic and leaf stability

analyses and created the figures, with input from M.F. T.N. calculated divergence estimates. S.G. and M.F. wrote the manuscript, with comments from all authors.

Author Information Reprints and permissions information is available at www.nature.com/reprints. The authors declare no competing financial interests. Correspondence and requests for materials should be addressed to sam.giles@earth.ox.ac.uk.

Methods

X-ray computed microtomography. IVPP V4096.6 and IVPP V4096.13 were scanned at IVPP, Chinese Academy of Sciences (CAS), Beijing, China, using a 225 kV microCT (developed by the Institute of High Energy Physics, CAS) at the following parameters: 150 kV, 100 μA, 720 projections, with a voxel size of 14.9 μA. *Erpetoichthys calabaricus* BMNH 2016.9.22.3 was scanned at King's College London with a voxel size of 8 μm. After scanning, data were segmented in Mimics (biomedical.materialise.com/mimics; Materialise, Leuven, Belgium). Surface meshes were then exported into and imaged in Blender (blender.org; Stitching Blender Foundation, Amsterdam, the Netherlands).

Phylogenetic analyses. Analyses were performed in PAUP* 4.01150[32] and MrBayes v.3.2.6[33]. The morphological-only dataset is based on ref. 27, but heavily expanded to incorporate additional Palaeozoic, Mesozoic and Recent taxa, as well as additional characters (both novel and drawn from the literature; see Character List for full references) with a bearing on their relationships. The resultant dataset comprises 265 characters and 93 taxa, and was analysed in PAUP* and MrBayes. A combined morphological and molecular dataset (with DNA sequences of 12 nuclear genes; only eight sampled for *Atractosteus*) was also analysed in MrBayes. Non-osteichthyan taxa were used in the outgroup and enforced with a constraint tree: [*Dicksonosteus*[*Entelognathus*[*Acanthodes*, *Cladodoides*, *Ozarcus*[ingroup]]]]. A small number of characters and incomplete taxa were excluded from the matrix of ref. 27. We assessed taxonomic equivalence[34] using Claddis[35], with no taxa found to be equivalent. Of the ten taxa coded for both morphological and molecular data in the

382 combined analysis, six are composites of more than one species, with three (two of
383 which are constrained in the outgroup, and one of which is a sarcopterygian) coded
384 from more than one genus, as follows: morphological data: *Cladodoides wildungesis*,
385 molecular data: *Leucoraja erinacea*; morphological data: *Ozarcus mapesae*,
386 molecular data: *Callorhinchus milli*; morphological data: *Miguashaia bureaui*,
387 molecular data: *Latimeria chalumnae*; morphological data: *Polypterus bichir*,
388 molecular data: *Polypterus senegalus*; morphological data: *Acipenser brevirostrum*,
389 molecular data: *Acipenser fulvescens*; morphological data: *Elops hawaiensis*,
390 molecular data: *Elops saurus*; *Erpetoichthys calabaricus*, *Lepisosteus osseus*, *Hiodon*
391 *alosoides* and *Amia calva* coded for both morphological and molecular data.
392
393 An equally weighted parsimony analysis in PAUP was conducted with 500 random
394 addition sequences, five trees held at each step, maxtrees set to automatically
395 increase, nchuck= 10 000, chuckscore= 1, and TBR enabled. Bootstrap values were
396 calculated in PAUP using 500 replicates of a heuristic search, with five trees held at
397 each step, rearrlimit= 50 000 000, limitperrep= yes, nchuck= 10 000, chuckscore= 1.
398 Bremer Decay values were calculated in PAUP.
399
400 Bayesian analyses was run under the *Mkv* model. Each dataset (i.e. combined
401 morphology and molecular and morphology only) was run until the standard deviation
402 of split frequencies reached less than 0.01, indicating convergence had been reached,
403 and this was confirmed in Tracer[36]. The first half of each run was discarded as burn-
404 in.
405

406 **Leaf stability**. Leaf stability was calculated using RogueNaRok[37], which utilises trees
407 generated during bootstrapping. Due to the computational limitations of
408 RogueNaRok, the 2554771 bootstrap trees were downsampled: random subsamples of
409 30 trees were generated using R[38], with maximum leaf stability then calculated for the
410 subset using the package ape[39]. This process was repeated ten times, with the average
411 maximum leaf stability plotted using the package geoscale[40] (Fig. 3a) and standard
412 deviation used as error (Extended Data Figure 10b). It may be expected that more
413 completely coded taxa will have higher leaf stability values by virtue of having lower
414 levels of anatomical uncertainty. To counter this, maximum leaf stability was
415 corrected for taxonomic incompleteness by calculating the residuals of a linear
416 regression between completeness and stability (Figure 3b, Extended Data Figure 10c).
417 The moving average was calculated by separating taxa (using midpoint of stage age)
418 into 25 Myr bins and calculating the average over two consecutive bins.
419

420 **Divergence estimates.** Divergence times of the sampled osteichthyan lineages were
421 estimated using the random local clock (RLC) model of molecular evolutionary rate
422 heterogeneity implemented in the computer program BEAST v. 1.8.1[41–43]. The
423 nucleotide substitution models were partitioned by gene and codon position for the 12
424 nuclear gene dataset, as in the MrBayes analysis above. A total of eighteen
425 exponential calibration priors from the fossil record of osteichthyans and
426 chondrichthyans were identified in the RLC analyses. As described in the text, the
427 first divergence time analysis used all calibrations, while the second held all aspects
428 of the analysis constant except for censorin all Palaeozoic-Triassic actinopterygian
429 calibrations. A birth-death speciation prior was used for branching rates in the
430 phylogeny. The BEAST analyses were run ten times and were combined using the

computer program LogCombiner v. 1.8.1 (http://beast.bio.ed.ac.uk/LogCombiner). Convergence of model parameter values and estimated node-heights to their optimal posterior distributions was assessed by plotting the marginal posterior probabilities versus the generation state in Tracer v. 1.6. Effective sample size (ESS) values were calculated for each parameter to ensure adequate mixing of the MCMC (ESS>200). The posterior probability density of the combined tree and log files was summarized as a maximum clade credibility tree using TreeAnnotator v. 1.8.1 (http://beast.bio.ed.ac.uk/TreeAnnotator). The mean and 95% highest posterior density estimates of divergence times and the posterior probabilities of inferred clades were visualized on the using the computer program FigTree v. 1.4.0 (http://beast.bio.ed.ac.uk/FigTree).

Methods References

33. Swofford, D. L. PAUP*: Phylogenetic Analysis Using Parsimony (*And Other Methods) v.4.0b 10 (Sinauer Associates, 2003).
34. Huelsenbeck J.P. & Ronquist F. MRBAYES: Bayesian inference of phylogeny. *Bioinformatics* 17: 754–755 (2011).
35. Wilkinson, M. Coping with missing entries in phylogenetic inference using parsimony. *Syst. Biol*. 44, 501–514 (1995).
36. Lloyd G.T. Claddis: an R package for performing disparity and rate analysis on cladistic-type data sets. (GitHub, https://github.com/graemetlloyd/Claddis, 2015).
37. Rambaut A, Suchard MA, Xie D & Drummond AJ (2014) Tracer v1.6, Available from http://beast.bio.ed.ac.uk/Tracer

38. R Core Team (2016). R: A language and environment for statistical computing. R Foundation for Statistical Computing, Vienna, Austria. URL https://www.R-project.org/.
39. Paradis E., Claude J. & Strimmer K. 2004. APE: analyses of phylogenetics and evolution in R language. Bioinformatics 20: 289-290.
40. Mark A. Bell. (2015). geoscale: Geological Time Scale Plotting. R package version 2.0. https://CRAN.R-project.org/package=geoscale
41. Aberer, A. J., Krompass, D. & Stamatakis, A. Pruning rogue taxa improves phylogenetic accuracy: an efficient algorithm and webservice. *Syst. Biol*. 62, 162–166 (2013).
42. Drummond, A.J. & Rambaut, A. BEAST: Bayesian evolutionary analysis by sampling trees. *BMC Evol. Biol.* 7, 214 (2007).
43. Drummond, A.J., Ho, S. Y. W., Phillips, M. J. & Rambaut, A. Relaxed phylogenetics and dating with confidence. *PLoS Biol.* 4:e88 (2006).

Data Availability

The CT data that support the findings of this study, as well as 3D surface files of described material, are available in figshare with the identifier https://doi.org/10.6084/m9.figshare.c.3814360. All other data files are included in the Supplementary Information.

Extended Data Figure Legends

Extended Data Figure 1 | Cranial anatomy of *Fukangichthys longidorsalis* based on high-resolution computed tomography. a, Lateral view of whole skull (IVPP V4096.13). **b,** Lateral view of braincase, hyomandibula and lower jaw (IVPP

V4096.6). **c,** Braincase in anterior view (IVPP V4096.6). **d,** Hyoid and branchial arches in dorsal view (IVPP V4096.13). **e,** Jaws and palate in ventral view (IVPP V4096.13). **f,** Left lateral view of whole skull (IVPP V4096.6). **g,** Right lateral view of whole skull (IVPP V4096.6). Abbreviations: asc, parasphenoid ascending process; av, accessory vomer; bb, basibranchial; bc, braincase; cb, ceratobranchial; chy, ceratohyal; clav, clavicle; clth, cleithrum; cor, coronoid process; den, dentary; dpal, dermopalatine; dsph, dermosphenotic; eb, epibranchial; hb, hypobranchial; hh, hypohyal; hmd, hyomandibula; ios, interorbital septum; jug, jugal; la, lachrymal; l.ex, lateral extrascapula; m.ex, median extrascapular; mx, maxilla; op, opercular process; opm, operculum; pb, pharyngobranchial; pq, palatoquadrate; proc, ectopterygoid process; prop, preopeculum; psp, parasphenoid; pt, posttemporal; qj, quadratojugal; so, suborbitals; sop, subopeculum; spcl, supracleithrum; sr, skull roof; II, optic foramen. Mouldic portion of lower jaw shaded. For a key to colours see Fig. 1. Scale bar, 5 mm in **a-b,d-g**, 2mm in **c**.

Extended Data Figure 2 | Photos of *Fukangichthys longidorsalis* specimens examined in this study. a, IVPP V4096.13 in left lateral view. **b,** IVPP V4096.13 in ventral view. **c,** IVPP V4096.13 in dorsal view. **d,** IVPP V4096.6 in left lateral view. **e,** IVPP V4096.6 in right lateral view. **f,** IVPP V4096.6 in dorsal view. Scale bar, 10 mm.

Extended Data Figure 3 | Interpretive drawings of comparative cranial anatomy of *Fukangichthys longidorsalis* (IVPP V4096.6 and IVPP V4096.13; a-e) and *Erpetoichthys calabaricus* (BMNH 2016.9.22.3; f-j) based on high-resolution computed tomography. a, Lateral view of whole skull (IVPP V4096.13). **b,** Lateral

view of braincase, hyomandibula and lower jaw (IVPP V4096.6). **c,** Braincase in anterior view (IVPP V4096.6). **d,** Hyoid and branchial arches in dorsal view (IVPP V4096.13). **e,** Jaws and palate in ventral view (IVPP V4096.13). **f,** Left lateral view of whole skull (IVPP V4096.6). **g,** Right lateral view of whole skull (IVPP V4096.6). Abbreviations: asc, parasphenoid ascending process; av, accessory vomer; bb, basibranchial; bc, braincase; cb, ceratobranchial; chy, ceratohyal; clav, clavicle; clth, cleithrum; cor, coronoid process; den, dentary; dpal, dermopalatine; dsph, dermosphenotic; eb, epibranchial; hb, hypobranchial; hh, hypohyal; hmd, hyomandibula; ios, interorbital septum; jug, jugal; la, lachrymal; l.ex, lateral extrascapula; m.ex, median extrascapular; mx, maxilla; op, opercular process; opm, operculum; pb, pharyngobranchial; pq, palatoquadrate; proc, ectopterygoid process; prop, preopeculum; psp, parasphenoid; pt, posttemporal; qj, quadratojugal; so, suborbitals; sop, subopercular; spcl, supracleithrum; sr, skull roof; II, optic foramen. Other abbreviations as in Fig. 1. Scale bar, 5 mm in **a-b,e-g,j**, 2mm in **c-d,h-i**.

Extended Data Figure 4 | Comparative palatal anatomy of *Fukangichthys longidorsalis* (IVPP V4096.6 and IVPP V4096.13; a-c,e) and *Erpetoichthys calabaricus* (BMNH 2016.9.22.3; **d,f) based on high-resolution computed tomography. a,** Medial view of left palate (IVPP V4096.13). **b,** Medial view of right palate (IVPP V4096.13). **c,** Medial view of left palate (IVPP V4096.6). **d,** Medial view of left palate. **e,** Anterolateral view of left palate (IVPP V4096.13). **e,** Anterolateral view of left palate. Abbreviations: av, accessory vomer; cor, coronoid process; dpal, dermopalatine; dmpt, dermometapterygoid; ect, ectopterygoid; ent, entopterygoid; proc, ectopterygoid process; mx, maxilla; qu, quadrate. Scale bar, 5 mm.

Extended Data Figure 5 | Comparative hyoid and branchial anatomy of *Fukangichthys longidorsalis* (IVPP V4096.6 and IVPP V4096.13; b-c,e-f,h-i,k-m) and *Erpetoichthys calabaricus* (BMNH 2016.9.22.3; **a,d,g,j) based on high-resolution computed tomography. Extended Data Figure 5 | Comparative hyoid and branchial anatomy of *Fukangichthys longidorsalis* (IVPP V4096.6 and IVPP V4096.13; b-c,e-f,h-i,k-m) and *Erpetoichthys calabaricus* (BMNH 2016.9.22.3**; **a,d,g,j) based on high-resolution computed tomography. a,** Braincase, palate, mandibular arch, hyoid arch and dorsal portion of branchial arch in ventral view. **b,** Braincase, palate, mandibular arch, hyoid arch and dorsal portion of branchial arch in ventral view (IVPP V4096.6). **c,** Braincase, palate, mandibular arch, hyoid arch and dorsal portion of branchial arch in ventral view (IVPP V4096.13). **d,** Ventral portion of hyoid and branchial arches in ventral view. **e,** Ventral portion of hyoid and branchial arches in ventral view (IVPP V4096.6). **f,** Branchial arches and ventral portion of hyoid arch in ventral view (IVPP V4096.13). **g,** Ventral portion of hyoid and branchial arches in dorsal view. **h,** Ventral portion of hyoid and branchial arches in dorsal view (IVPP V4096.6). **i,** Branchial arches and ventral portion of hyoid arch in ventral view (IVPP V4096.13). **j,** Hyoid arch and ventral portion of branchial arches in lateral view. **k,** Hyoid arch and ventral portion of branchial arches in lateral view (IVPP V4096.6). **l,** Hyoid and branchial arches in lateral view (IVPP V4096.13). **m,** close-up of uncinated process of epibranchial. Abbreviations: ahy, groove for afferent hyoid artery; bb, basibranchial; cb, ceratobranchial; chy, ceratohyal; eb, epibranchial; hb, hypobranchial; hh, hypohyal; hmd, hyomandibula; ih, interhyal; op, opercular process; psp, parasphenoid; up, uncinate process. For a key to colours see Fig. 1. Scale bar in **a**-**l**, 5 mm; in **m**, 1 mm.

Extended Data Figure 6 | Results of phylogenetic analyses. a, Strict consensus of the 14450 shortest trees (1347 steps) for 93 taxa and 265 equally weighted characters. Digits above nodes indicate Bremer decay indices above 1. Digits below nodes indicate percentage bootstrap support above 50%. **b,** Adams consensus tree of the 14450 shortest trees (1347 steps) for 93 taxa and 265 equally weighted characters. Scanilepids and polypterids bolded.

Extended Data Figure 7 | Results of phylogenetic analyses. Agreement subtree of the 14450 shortest trees (1347 steps) for 93 taxa and 265 equally weighted characters. Scanilepids and polypterids bolded. 78 of 93 taxa are included, and the following taxa are pruned from the tree: *Beagiascus pulcherrimus*, *Beishanichthys brevicaudalis*, *Birgeria groenlandica*, *Cosmoptychius striatus*, *Cyranorhis bergeraci*, *Guiyu oneiros*, *Howqualepis rostridens*, *Lawrenciella schaefferi*, *Mimipiscis toombsi, Onychodus jandemarrai*, *Platysomus superbus*, *Psarolepis romeri*, *Scanilepis dubia*, *Tanaocrossus kalliokoskii*, *Wendyichthys dicksoni*.

Extended Data Figure 8 | Results of Bayesian analyses. a, Combined morphological and molecular dataset. Terminals in blue are coded for both molecular and morphological data. Scanilepids and polypterids bolded. **b,** Morphological only dataset. Numbers at nodes represent posterior probability support; asterisks represent a posterior probability of 1.

Extended Data Figure 9 | Endocast and bony labyrinth of *Erpetoichthys calabaricus* (BMNH 2016.9.22.3) showing vestigial lateral cranial canal. a, Dorsal

view. **b,** lateral view. **c,** Transverse tomograph through otic region. Abbreviations: a.amp, ampulla of the horizontal anterior semicircular canal; hsc, horizontal semicircular canal; lcc, lateral cranial canal; psc, posterior semicircular canal. Scale bar, 5 mm.

Extended Data Figure 10 | Leaf stability analyses. a, Raw leaf stability plotted against taxon age (same plot as in Main Text Figure 3a). **b**, Raw leaf stability plotted against taxon age. Error bars represent standard deviation (same plot as in Main Text Figure 3a). **c**, Residuals from a linear regression of stability against taxon incompleteness, plotted against taxon age (same plot as in Main Text Figure 3b). Taxa identified in Supplementary Table 2.